Organic-template-directed nucleation of strontium fluoride and barium fluoride: Epitaxy and strain

Jan Kmetko,* Chungjong Yu, Guennadi Evmenenko, Sumit Kewalramani, and Pulak Dutta[†]

Department of Physics and Astronomy, Northwestern University, Evanston, Illinois 60208, USA

(Received 8 January 2003; published 28 August 2003)

In situ synchrotron x-ray diffraction studies show that barium and strontium fluoride grow preferentially oriented at a fatty-acid monolayer template, with the unit cell spacings initially contracted by ~1.6% (SrF_2) to ~4% (BaF_2). In addition to this macroscopic strain, peak width analysis shows the presence of local strain that relaxes as the crystals grow. In contrast, the diffraction pattern from calcium carbonate grown at the same template shows no preferred crystallographic orientation.

I. INTRODUCTION

The use of inorganic templates to direct the growth of inorganic films (typically under ultrahigh vacuum) is by now a major industry, and inorganic templates are also used to grow structured organic thin films (such as self-assembled films). In nature, however, it is more common to use organic templates to grow inorganic crystals, a process known as biomineralization. Organic template-directed nucleation is a new and potentially easier way to grow tailored inorganic materials, but our understanding of such processes is at a relatively early stage.

The best-studied class of organic-template-mediated nucleation processes is the growth of oriented crystals under organic monolayers (Langmuir films) that have been spread at air/supersaturated-solution interfaces.[1–7] The weakly acidic headgroups of the organic molecules attract aqueous ions of metal salts to the water surface, where the ions aggregate in large concentrations and grow into crystals. In contrast to the uncontrolled precipitation of a salt from an aqueous solution, here the crystallites grow preferentially oriented to the plane of the organic template, and have specific morphology and size. The matrix-mediated-growth of crystals such as $CaCO_3$,[8–12] CaC_2O_4,[13] $BaSO_4$,[14–16] KH_2PO_4,[17] BaF_2,[18,19] CdS,[20] and PbS[21,22] have been studied, mostly by various *ex situ* methods—the crystals are removed from the solution and examined by optical, transmission electron, scanning electron, Brewster angle, and atomic force microscopies; x-ray photoelectron spectroscopy; energy-dispersive x-ray analysis; electron and x-ray diffraction; etc. A wealth of information has been accumulated about the organic monolayer material and subphase conditions best suited for nucleation of a particular mineral in a particular orientation.

None of the above-referenced studies, however, provide information at the microscopic level. The popular (and reasonable) explanation[23] for the preferentially oriented inorganic nucleation at the organic template is that it stems from a match between the interfacial lattices of the organic molecules and inorganic molecules. Such interfacial organic-inorganic registry has recently been sought using grazing incidence diffraction (GID) on the growth of a calcium carbonate film under Langmuir monolayer of arachidic acid,[24] on oriented crystal growth of glycine under Langmuir monolayers of α-amino acids,[25] and on the growth of oriented ice under alcohol monolayers.[26,27] In the case of calcium carbonate,[24] only amorphous growth was observed. In the other studies, no linear relationship between the organic and inorganic lattices has been determined. In our recent GID study[28] of barium fluoride nucleation under monolayers of heneicosanoic acid, we reported that the interfacial organic and inorganic lattices do achieve a precise registry. This happens only because both the organic molecules and the inorganic atoms rearrange as needed at the initial stage of growth.

In this paper, we address two experimental issues. First, we test whether the organic monolayer has a similar effect on two other minerals, strontium fluoride, and calcium carbonate. Strontium fluoride was chosen not only because it is isostructural with barium fluoride, but also because it possesses properties desirable for crystal growth from solution: it forms no intermediate polymorphs, it has no stable hydrates, it has a low solubility, and its supersaturated solution can be prepared by chemical reactions. We chose calcium carbonate because it and its polymorphs are biologically important and therefore have been extensively studied.

Second, we analyze diffraction peak widths to obtain information on the domain sizes and structural defects during the initial stage of growth. Structural defects can play an important role during an epitaxial growth. For example, inorganic crystals are known to grow on inorganic substrates preferentially oriented, even if the surface lattices of the substrate and deposited material are substantially (as much as 30%) mismatched.[4] In such cases, the lattices cannot distort to accommodate a one-to-one fit; instead, the initially formed overlayers contain structural defects that accommodate the strain energy associated with the lattice misfit. Such crystal defects, in addition to causing the diffraction peaks to shift, contribute to the broadening of diffraction peaks.

II. EXPERIMENTAL DETAILS

Supersaturated aqueous solutions of strontium fluoride were prepared at concentrations of 4.5 and 7.5 mM by mixing appropriate stoichiometric amounts of strontium chloride and ammonium fluoride, and supersaturated solutions of calcium carbonate were prepared at concentrations of 7 and 20

mM by mixing stoichiometric amounts of calcium chloride (dihydrate) and sodium bicarbonate (Sigma, quoted purity 99.99% or better for all salts). The pH was adjusted with sodium hydroxide (Sigma, quoted purity 99.998%) to 8.0 and measured in the beaker before the solutions were poured into the trough. About 65 mL of a 0.87 mg/mL solution of heneicosanoic acid ($C_{20}H_{41}COOH$, or C_{21}, Sigma, quoted purity 99%) in chloroform was spread on pure water once and compressed by a mechanical barrier in order to determine the area (A_0) corresponding to the pressure only very slightly above 0 dynes/cm. The surface pressure (π) was measured with ± 0.5 dyne/cm accuracy (Balance ST9000, Nima Technology). In subsequent sample preparations, the same amount of the fatty acid was spread on the aqueous salt solutions at constant area A_0 at 25 °C (the barrier was not moved so that the organic film and the process of inorganic nucleation were not disturbed). A slight overpressure of helium was maintained in the trough to reduce radiation damage and air scattering.

The experimental setup and procedures for data collection were similar to those described elsewhere.[29] GID studies of films with calcium were performed at the 1-BM-C (bending magnet) beamline of SRI-CAT at the Advanced Photon Source, Argonne National Laboratory and studies of films with strontium were performed at the X-14A beamline (Oak Ridge National Laboratory Beamline, bending magnet) at the National Synchrotron Light Source, Brookhaven National Laboratory. The wavelength of the beam ($\lambda = 1.5491$ Å) was the same at both beamlines. Vertical and horizontal soller slits in front of the detector defined a horizontal resolution of ~ 0.01 Å^{-1} full width at half maximum (FWHM) for K_{xy} scans and a vertical resolution of ~ 0.05 Å^{-1} FWHM for K_z scans. Two scintillation detectors were used to monitor the intensities of the beam incident on the water surface and specularly reflected from it.

III. LINE SHAPE ANALYSIS

Lattice distortions in a crystal can be either uniform (macrostrain) or nonuniform (microstrain). Both "macrostrain" and "microstrain" refer to the *microstructure* of the crystallites.[30] The uniform lattice distortions are residual stresses that cause lattice spacings to expand or contract, and thus shift the diffraction peaks in the reciprocal space. In the case of nonuniform lattice distortions, the crystal lattice spacings range between $d - \Delta d$ and $d + \Delta d$,[31] and this causes broadening of the diffraction line shapes. The peak profiles will also be broadened by the instrumental resolution and by the finite crystallite size. The objective of the analysis is to separate out the contribution to the broadening from the effects of instrumental resolution, size, and strain. We use simplified integral breadth methods[32] to estimate information about the size of crystallites and the effect of microstrain. We label the integral breadths of the profiles from size, distortion (strain), and instrumental resolution as $(\delta K_{xy})^S$, $(\delta K_{xy})^D$, and $(\delta K_{xy})^R$, respectively. The integral width $(1/I_p)\int I(K)dK$ is the width of a rectangle having the same area and peak height as the fitted Gaussian line profile; this is
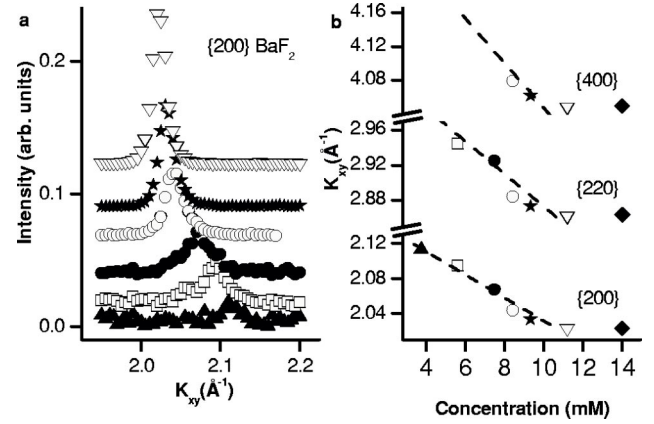

FIG. 1. Macrostrain relaxation in barium fluoride at the mineral-matrix interface as a function of solution concentration (reproduced from Ref. 28). The peak positions have been determined with an accuracy of ± 0.002 Å^{-1} (smaller than the data symbols). The peaks also shift with time, but much more slowly than for strontium fluoride (below).

a convenient measure because the Scherrer formula for line width due to finite size becomes simply

$$(\delta K_{xy})^S = \frac{2\pi}{L} \tag{1}$$

with no other constants. L is the effective crystalline dimension, or more precisely, the volume average of the mean crystallite dimension. The integral profile breadth due to distortions (microstrain) alone may be expressed as

$$(\delta K_{xy})^D = 2\left(\frac{\Delta d}{\bar{d}}\right)K_{xy}, \tag{2}$$

where the parameter ($\Delta d/\bar{d}$) is a measure of the microstrain. The breadth for the instrumental resolution function $\delta(2\theta_{xy})^R$ was determined experimentally from a silicon powder standard, and $(\delta K_{xy})^R$ calculated from this measurement for the K_{xy} values of interest. We assume that the three broadening effects give Gaussian lineshapes, so that when all three effects are present, $(\delta K_{xy})_0^2 = [(\delta K_{xy})^S]^2 + [(\delta K_{xy})^D]^2 + [(\delta K_{xy})^R]^2$.

IV. RESULTS

A. Macrostrain

For BaF$_2$, it is known[18,19] that nucleation from solution at a Langmuir monolayer occurs with a preferred orientation, the (00*l*) axis being normal to the water surface. Our studies of BaF$_2$ nucleation have been described in a recent paper.[28] In brief, we find that the horizontal lattice spacings and the inorganic film thickness depend on solution concentration, with the least supersaturated solutions forming the most distorted layers (Fig. 1). As expected, the distortion occurs in very thin layers (14 Å for 5.6 mM solutions, estimated from the widths of Bragg rods shown in Fig. 3 of Ref. 28). The vertical lattice spacings cannot be determined with any precision because the peaks are wide in the z direction. At the dilute limit, the square inorganic lattice and the oblique or-
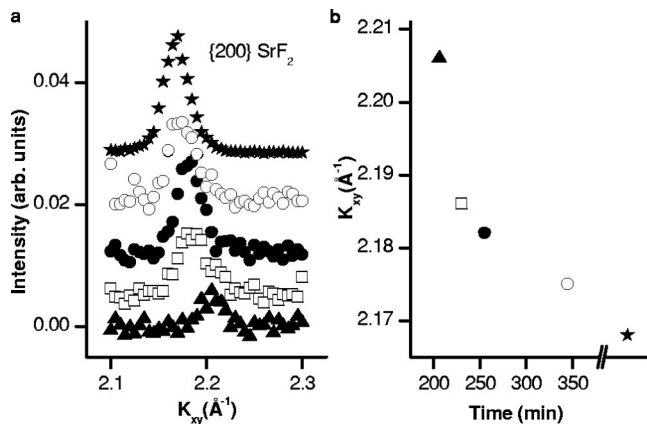
FIG. 2. Macrostrain relaxation in strontium fluoride at the mineral-matrix interface. (a) A representative {200} diffraction peak "shifts" as a function of time at concentration of 4.5 mM. The following symbols denote time after spreading the organic film: ▲ 206 min, □ 230 min, ● 255 min, ○ 345 min. The peak from a slightly more concentrated solution (7.5 mM) denoted by a star appears at the ideal, bulk position immediately. (b) The {200} peak position as a function of time. The mineral is initially strained by ~1.6% from its bulk structure. The peak positions have been determined with an accuracy of ± 0.002 Å^{-1} (smaller than the data symbols).
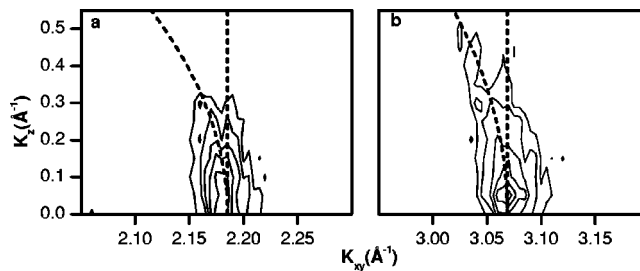

FIG. 3. Intensity contours from strontium fluoride diffraction peaks at low supersaturation, 4.5 mM. (a) The {200} contour is partially smeared out in the out-of-plane direction along a Bragg rod and partially along a Debye ring. The dashed lines along the two directions of smearing are guides to the eye. (b) The same combination of effects is seen in the {220} contour.

ganic lattice are commensurate, with the unit cell areas being in a ratio of 1.50 to 1. At a given concentration, the BaF$_2$ lattice spacings will relax towards the unstrained values with time, but very slowly. It is therefore more convenient to use solution concentration to vary the BaF$_2$ layer thickness and thus the macroscopic strain.

We have subsequently studied the nucleation of SrF$_2$. A weak {200} peak of strontium fluoride appears from a barely supersaturated solution (4.5 mM) about 3 h after the sample preparation, but at a higher K-vector position than expected from an ideal crystal. Successive scans of this peak show that it is shifting toward the bulk position with time as shown in Figs. 2(a) and 2(b). The peak position reaches a value close to that of the bulk structure about 6 h after the sample preparation. The in-plane {220} and {400} peaks have also shifted to higher than bulk positions. In other words, the mineral nucleates with a strained cubic lattice at the initial stage, with the horizontal unit-cell spacing contracted from its bulk value of 5.8 Å by 1.6%, and the strained structure relaxes toward the bulk unit-cell with time. This is the same effect of lattice contraction induced by the organic monolayer as we have previously reported for barium fluoride, but at the same supersaturation, the average rate of SrF$_2$ peak shifts (-2×10^{-4} Å^{-1}/min) is much faster than that of previously observed BaF$_2$ peak shifts (-5×10^{-5} Å^{-1}/min). This is consistent with the known fact that, on average, the nucleation rate of bulk strontium fluoride[33] is faster than that of a bulk barium fluoride.[34] The relatively fast relaxation of strontium fluoride, unfortunately, means that we cannot track the corresponding reorganization of molecules in the organic layer, which we were able to do with barium fluoride.[28] We do see the LS-phase diffraction peaks at undersaturated concentrations (not shown) just as we have seen with other divalent

ions[35] in dilute solutions. Because of the narrow metastable region of strontium fluoride, diffraction peaks (designated by a star in Fig. 2) from slightly more concentrated solutions appear at their usual bulk position immediately after spreading the organic film.

The contour plots in Figs. 3(a) and 3(b) at low supersaturation show that the {200} and {220} Bragg spots for SrF$_2$ are smeared partly along a vertical line (Bragg rod), and partly along Debye rings. These two directions of smearing indicate that the bulk inorganic crystals grow from a thin inorganic layer into slightly misoriented crystallites. The width of the Bragg rods indicate that the inorganic layer is less than 20 Å thick when the solution concentration is 4.5 mM. Just as in the case of BaF$_2$, the lattice spacings in the z direction cannot be precisely determined because peaks are so wide. At high supersaturation (7.5 mM), the diffracted intensity is not distributed along Bragg rods but entirely along the Debye rings (Fig. 4). Intensity variations along {$hk0$} rings have their maxima at $K_z \sim 0$ Å^{-1} (in the plane of water), and al-
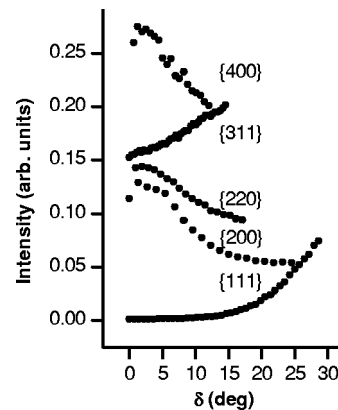

FIG. 4. At high supersaturation (7.5 mM), the diffracted intensity is entirely peaked along the Debye rings. The maxima of the intensity distribution indicate that the strontium fluoride crystallites are preferentially oriented with the ⟨001⟩ face parallel to the plane of the water surface. The angle δ is defined as $\tan \delta = |K_z|/|K_{xy}|$; the total wave vector $K = \sqrt{K_{xy}^2 + K_z^2}$ is the radius of the Debye ring. Intensity values for data points of the {111} curve have been divided by 50 and for the {200} and {311} curve by 5 so that they can be shown on the same scale.
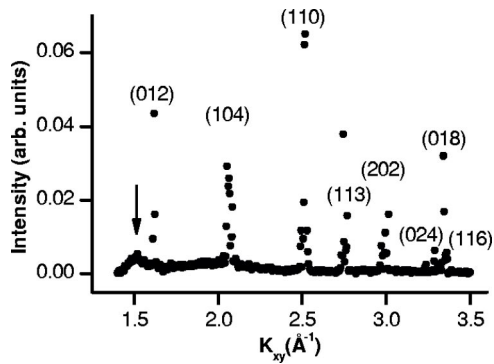
FIG. 5. An in-plane ($K_z = 0$) diffraction scan of interfacial calcium carbonate. All allowed peaks of calcite are visible, indicating that there is no preferred crystallographic orientation. In contrast to the nucleation of fluorides, the growth of calcium carbonate leaves the organic peak unchanged (see arrow).

though our apparatus does not allow us to scan far enough to observe the maxima of the off-plane $\{hk1\}$ rings, it is apparent that the $\langle 001 \rangle$ face of bulk strontium fluoride lies parallel to the plane of the organic matrix. We do not see evidence of other epitaxial orientations or of any unoriented crystallites. Based on the intensity variations along the rings, the extent of misorientation is only $\pm 5°$ FWHM at 7.5 mM.

Motivated by numerous, nonstructural studies of the oriented nucleation of the biologically important calcium carbonate, we have also looked for the face-selective nucleation of this salt. Consistent with previous macroscopic studies,[11] we see that calcium carbonate nucleates at the air-water interface in the form of either vaterite or calcite, depending on calcium concentration in the subphase. However, our studies show that neither of the two polymorphs have a preferred crystallographic orientation; they both nucleate as powders, as shown in the representative in-plane diffraction scan of
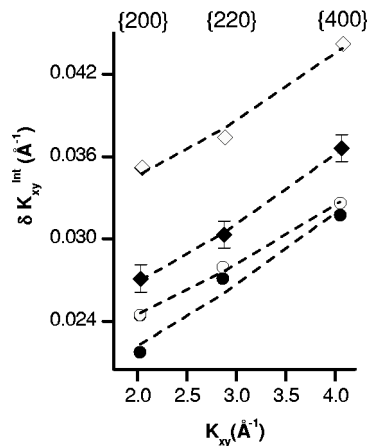
calcite in Fig. 5. As expected from a powder, all allowed calcite peaks are visible in a horizontal radial scan, regardless of the crystallographic indices. Also as expected from unoriented crystallites, the intensity along Debye rings (not shown) fluctuates unpredictably. It is possible that there is a small number of oriented calcite crystals that are not seen by our x-ray beam because their orientation about the vertical axis never satisfies the diffraction condition. Other than that, we cannot explain the discrepancy between our *in situ* and previous *ex situ* studies by others.[11]

The arrow in Fig. 5 points to a peak from the *LS* phase of the organic monolayer that is also seen with other ions at undersaturated concentration. Although the organic *LS* peak disappears at supersaturated concentrations of fluorides after crystals nucleate, it is unaffected by nucleation of calcium carbonate.

B. Microstrain

When barium and strontium fluoride are grown at an organic template, there is a lattice parameter distortion, resulting in shifts of the diffraction line positions. The diffraction peaks of strontium fluoride are weak and shift continuously with time, so their width cannot be ascertained with sufficient precision. However, we have measured and analyzed the broadening of barium fluoride diffraction peaks.

Peaks at all concentrations are broader than the resolution limit of about 1000 Å. As can be seen in Fig. 6, the integral
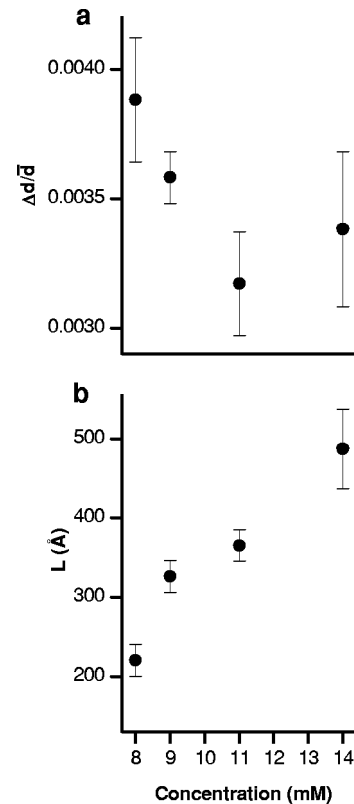

FIG. 6. Integral widths of the diffraction peaks from interfacial barium fluoride. The following symbols denote the salt concentration (in mM): ● 14.0, ○ 11.2, ◆ 9.3, ◇ 8.4. If the peak broadening were solely due to finite lateral size, the widths would be independent of the scattering vector. In fact, the width depends on the scattering vector, and also increases as the concentration decreases. The broadening is thus most likely caused by an increased number of structural defects at the earlier stages of growth.

FIG. 7. Strain relaxation in barium fluoride at the mineral-matrix interface. The microstrain parameter ($\Delta d / \bar{d}$) and the domain size L have been determined from fits to the peak widths shown in Fig. 6.

breadth of diffraction lines depends on K_{xy}; thus, the finite size effect [Eq. (1)], which predicts a width that depends on L only, is not the only source of peak broadening. We fit the trends as discussed earlier, and extract the in-plane domain size L and strain parameter ($\Delta d/\bar{d}$) [as shown in Eq. (2)]. L is about 200 Å at low concentrations, and as the crystallites grow (at higher concentrations), L increases up to about 500 Å [Fig. 7(b)]. Although the microstrain remains present even after the peak positions approach their ideal, bulk values, it decreases slightly as the domain size increases [Fig. 7(a)]. There are thus three different events occurring simultaneously: the inorganic crystals grow laterally (as well as transversely); their crystal structure relaxes uniformly (the peaks shift back to their bulk positions); and the nonuniform spread in the spacings reduces slightly. These trends are consistent with the expectation that the structure approaches the nonstrained form as the crystallites grow.

Our observations reveal global strain effects (peak shifts) that are correlated with increasing microstrain (peak broadening) at the organic-inorganic interface. Strain in solid materials can be associated with many different types of crystal defects, but generally, it is not possible to distinguish between these effects from diffraction data. Given the nature of our sample, it is likely that there is entrapment of water or hydroxyl ions within the crystal.

V. CONCLUSIONS

Strontium fluoride, similar to barium fluoride, begins to nucleate with a strained structure at the organic-inorganic interface and grows with its $\langle 001 \rangle$ crystallographic face preferentially oriented to the plane of the water surface. Calcium carbonate, on the other hand, grows with no preferred crystallographic orientation. We conclude that the cubic unit cells of the fluorides possess the symmetry and lattice parameters necessary for the registry at the heneicosanoic acid template. In addition to peak shifts, strong peak broadening effects from metastable supersaturated solutions of barium fluoride can be attributed to microstrain, which is highest when the macrostrain is highest. The broadening indicates that the initial inorganic nuclei form with a higher density of point defects. As the crystals grow, the density of defects decreases. The structural defects in the initial stage presumably account for the flexibility of the inorganic lattice, and allow commensurate ordering of inorganic atoms at the structured organic interface.

*Present address: Department of Physics, Cornell University, Ithaca, NY 14583, USA.

†Electronic address: pdutta@northwestern.edu

[1] S. Mann, in *Inorganic materials*, edited by D.W. Bruce and D. O'Hare (Wiley, Chichester, England, 1992), p. 238.

[2] S. Mann, Nature (London) **365**, 499 (1993).

[3] S. Mann, D.D. Archibald, J.M. Didymus, T. Douglas, B.R. Heywood, F.C. Meldrum, and N.J. Reeves, Science **261**, 1286 (1993).

[4] S. Mann, *Biomineralization: Principles and Concepts in Bioinorganic Materials Chemistry* (Oxford University Press, New York, 2001).

[5] H. Rapaport, I. Kuzmenko, M. Berfeld, K. Kjaer, J. Als-Nielsen, R. Popovitz-Biro, I. Weisbuch, M. Lahav, and L. Leiserowitz, J. Phys. Chem. B **104**, 1399 (2000).

[6] I. Weissbuch, R. Popovitz-Biro, M. Lahav, and L. Leiserowitz, Acta Crystallogr., Sect. B: Struct. Sci. **51**, 115 (1995).

[7] M. Lahav and L. Leiserowitz, J. Phys. D **26**, B22 (1993).

[8] B.R. Heywood and S. Mann, Chem. Mater. **6**, 311 (1994).

[9] A. Litvin, S. Valiyaveettil, D. Kaplan, and S. Mann, Adv. Mater. (Weinheim, Ger.) **9**, 124 (1997).

[10] S. Mann, B. Heywood, S. Rajam, and J. Walker, J. Phys. D **24**, 154 (1991).

[11] J.B. Walker, B.R. Heywood, and S. Mann, J. Mater. Chem. **1**, 889 (1991).

[12] G. Xu, N. Yao, I. Aksay, and J. Groves, J. Am. Chem. Soc. **120**, 11977 (1998).

[13] R. Backov, C.M. Lee, S.R. Khan, C. Mingotaud, G.E. Fanucci, and D.R. Talham, Langmuir **16**, 6013 (2000).

[14] B.R. Heywood and S. Mann, Adv. Mater. (Weinheim, Ger.) **4**, 278 (1992).

[15] B.R. Heywood and S. Mann, Langmuir **8**, 1492 (1992).

[16] B.R. Heywood and S. Mann, J. Am. Chem. Soc. **114**, 4681 (1992).

[17] B. Li, Y. Liu, N. Lu, J. Yu, Y. Bai, W. Pang, and R. Xu, Langmuir **15**, 4837 (1999).

[18] L. Lu, H. Cui, W. Li, H. Zhang, and S. Xi, J. Mater. Res. **16**, 2415 (2001).

[19] L. Lu, H. Cui, W. Li, H. Zhang, and S. Xi, Chem. Mater. **13**, 325 (2001).

[20] J. Yang, F.C. Meldrum, and J.H. Fendler, J. Phys. Chem. **99**, 5500 (1995).

[21] J. Yang and J.H. Fendler, J. Phys. Chem. **99**, 5505 (1995).

[22] X. Zhao, J. Yang, L. McCormick, and J. Fendler, J. Phys. Chem. **96**, 9933 (1992).

[23] S. Mann, in *Biomineralization: Chemical and Biochemical Perspectives*, edited by S. Mann, J. Webb, and R. J. Williams (VCH, New York, 1989).

[24] E. DiMasi, V. Patel, M. Sivakumar, M. Olszta, Y. Yang, and L. Gower, Langmuir **18**, 8902 (2002).

[25] I. Weissbuch, M. Berfeld, W. Bouwman, K. Kjaer, J. Als-Nielsen, M. Lahav, and L. Leiserowitz, J. Am. Chem. Soc. **119**, 933 (1997).

[26] J. Majewski, R. Popovitz-Biro, K. Kjaer, J. Als-Nielsen, M. La-

hav, and L. Leiserowitz, J. Phys. Chem. **98**, 4087 (1994).

[27] J. Majewski, L. Margulis, D. Jacquemain, F. Leveiller, C. Böhm, T. Arad, Y. Talmon, M. Lahav, and L. Leiserowitz, Science **261**, 899 (1993).

[28] J. Kmetko, C.-J. Yu, G. Evmenenko, S. Kewalramani, and P. Dutta, Phys. Rev. Lett. **89**, 186102 (2002).

[29] S. Barton, B. Thomas, E. Flom, S. Rice, B. Lin, J. Peng, J. Ketteron, and P. Dutta, J. Chem. Phys. **89**, 2257 (1988).

[30] G. Kimmel and D. Dayan, in *Defect and Microstructure Analysis by Diffraction*, edited by R. Snyder, J. Fiala, and H. Bunge (Oxford University Press, Oxford, 1999).

[31] J. Langford, in *Defect and Microstructure Analysis by Diffraction*, edited by R. Snyder, J. Fiala, and H. Bunge (Oxford University Press, Oxford, 1999).

[32] H. P. Klug and L. E. Alexander, *X-ray Diffraction Procedures for Polycrystalline and Amorphous Materials* (Wiley, New York, 1974).

[33] R. Bochner, A. Abdul-Rahman, and G. Nancollas, J. Chem. Soc., Faraday Trans. 1 **80**, 217 (1984).

[34] J. Barone, D. Svrjcek, and G. Nancollas, J. Cryst. Growth **62**, 27 (1983).

[35] J. Kmetko, A. Datta, G. Evmenenko, and P. Dutta, J. Phys. Chem. B **105**, 10818 (2001).